Polymer Degradation and Stability xxx (xxxx) xxx

Contents lists available at ScienceDirect

Polymer Degradation and Stability

journal homepage: www.elsevier.com/locate/polymdegradstab

Evaluating poly(ether ether ketone) powder recyclability for selective laser sintering applications

Akanksha Patel[a], Varun Venoor[a], FeiFei Yang[b], Xu Chen[b], Margaret J. Sobkowicz[a,*]

[a] Department of Plastics Engineering, University of Massachusetts, Lowell, MA, 01854, USA
[b] Department of Mechanical Engineering, University of Washington, Seattle, WA, 98195, USA

ARTICLE INFO

Article history:
Received 27 August 2020
Revised 19 January 2021
Accepted 26 January 2021
Available online xxx

ABSTRACT

Poly(ether ether ketone) (PEEK) is increasingly used in selective laser sintering (SLS) due to its superior mechanical and thermal properties and biocompatibility. It is well known that the properties of selective laser sintering (SLS) powder govern the processability and quality of the parts. The SLS printing process exposes the PEEK bed/feedstock to variable elevated temperatures (above 300 °C) for a prolonged time. The effect of this thermal history on the part quality is unknown. This work evaluates the changes that occur in thermally treated PEEK powder through spectroscopic, morphological, and rheological characterizations. It was found that crystallinity increased marginally within the first two hours, but particle size and shape remained virtually unchanged. The thermal treatment also resulted in a significant increase in the melt viscosity of the PEEK powder, and its flowability slightly improved. Understanding these changes could help to reduce waste through recycling of some portion of PEEK powders used in SLS printing.

1. Introduction

3D printing or additive manufacturing (AM) was developed in the 1980s by Charles Hull [1]. This technique has provided flexibility to use a broad range of materials for many end-use applications, for example, electronics [2], medical devices, automobile parts, and aerospace. This process leads to a fast, customizable, and cost-effective production [3]. Stereolithography (SLA), selective laser sintering (SLS), and fused filament fabrication (FFF) are three main AM technologies for plastic part manufacturing and fabrication. SLA requires light-activated polymers to prepare the layers of a part and an UV energy source to cure it. [4]. SLS is a powder-based technique, where a bed of thermoplastic powder is deposited on the platform, and subsequent tracing of the powder is conducted by a heat source (e.g., carbon dioxide laser) to melt and fuse the powder under controlled conditions [5–7]. The SLS process was developed to solve the limitations of other AM techniques but its high-cost instrumentation and waste of powder feedstock are still challenges for commercialization. The most common materials used in SLS are polyamide (PA-11, PA-12), poly(ethylene terephthalate) (PET), and poly(ether ether ketone) (PEEK), for SLS.

PEEK is a semi-crystalline thermoplastic that is well known for its outstanding thermal, chemical, and mechanical properties; it is also resistant to chemicals, oxidation, and radiation [8,9]. PEEK (Fig. 1) properties vary according to molecular structure and molecular weight distribution [10]. The crystalline portion of the polymer mainly determines the mechanical, thermal, and rheological properties of the end products; higher crystalline fraction provides a broader melting temperature range, higher modulus, and strength with lower toughness and flexibility [11]. PEEK is most suitable for high-performance applications including aircraft and automobile parts such as bearings, pistons, and pumps. It has also found use in biomedical devices such as orthopedic implants [12,13]. PEEK has a comparatively high melt temperature (343 °C) and high viscosity at moderate temperatures; thus, it is difficult to process PEEK through other methods [14,15]. Inherent material properties like particle size distribution, crystallinity, powder flowability, melting temperature, and melt viscosity affect the final part quality, and process parameters such as raster rate and path, laser power, and ambient bed temperature also play important roles during SLS processing [16,17].

In powder bed SLS, poor flowability leads to inhomogeneous and uneven layers, which results in porous and weak parts [18,19]. Flowability is dictated by various factors: powder properties (particle shape, size, and its distribution [PSD], surface features), environmental constraints (relative humidity, temperature), and test method adopted [20,21]. Build layer thickness in SLS should be

* Corresponding author.
E-mail addresses: margaret_sobkowiczkline@uml.edu, sobko100@hotmail.com (M.J. Sobkowicz).

https://doi.org/10.1016/j.polymdegradstab.2021.109502
0141-3910/

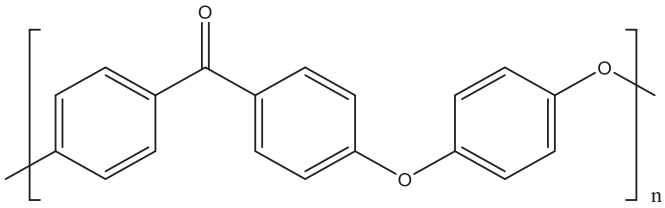

Fig. 1. Chemical structure of poly(ether ether ketone) (PEEK) polymer.

maintained at a minimum of two times the average particle size (μm) [18]. Chung and Das [22] asserted the preferred range of particle size range to be 10–150 μm. Particle size is also known to control laser penetration depth during SLS [23]. Berretta et al. [24] examined morphology, inter-particle interactions, and flowability of new commercially available PEEK powders. PEEK 450PF (Victrex®) was found to be the least spherical, with angle of repose (AOR) of 52.8° for neat powder suggesting poor flowability, which was marginally improved using particulate fillers such as calcium carbonate ($CaCO_3$); a 70:30 mixture of 450PF/ $CaCO_3$ exhibited better flowability with measured AOR of 48.2°.

Jonas and Legras [25] investigated the degradation phenomenon and induced crystallization behavior in PEEK. The three aromatic/phenyl rings present in the structure can be converted into aliphatic/linear chains to some degree by a ring-opening mechanism [26]. The presence of linear chain segments eventually decreases thermal stability or reduces the melting point of PEEK [27]. PEEK's thermal decomposition mainly starts with random homolytic scission of ether or carbonyl bonds. The atmospheric composition (i.e., presence of oxygen) also changes the decomposition rate of PEEK, which usually starts around 500 °C. Oxidative degradation products include carbon monoxide (CO), carbon dioxide (CO_2), phenols, and some aromatic ethers [28]. Thermal degradation of PEEK has been studied using step pyrolysis (in the absence of oxygen), which shows selective cleavage of polymer chains by the extraction of 4-phenoxyphenol and 1,4-diphenoxybenzene at 450 °C [29].

Oxidation of PEEK is known to occur on the hydrocarbon groups present in the aromatic rings, as determined using Fourier transform infrared spectroscopy (FTIR) [25]. Above 400 °C, oxidation is a result of the splitting of ether ketone bonds present in the monomer unit [25,28,30–32]. FTIR has also been used to follow the decrease of the ketone peak at 1653cm^{-1} and formation of several degradation products such as phenols (3400 to 3700cm^{-1}), phenyl benzoate (1739 cm^{-1}), fluorenone (1711 cm^{-1}) [25,28,32]. PEEK is also known to undergo degradation predominately due to chain scission between 300 and 485 °C [28,30,31,33]. The mechanism of crosslinking is reported to be from the bimolecular recombination of phenyl radicals.

The rheological behavior of SLS polymers such as polyamide and PEEK is known to influence powder fusion and coalescence [34–36]. The sintering process of powder-based materials was described by a viscous model deduced by Frenkel [37]. Eq. (1) relates process parameters with powder properties such as surface tension and melt viscosity [34]:

$$\frac{x}{r} = \left(\frac{3\gamma}{2\eta_0 r}\right)^{1/2} t^{1/2} \tag{1}$$

In Eq. (1) x represents the particle coalescence length relative to particle radius (r), γ is the surface tension (N/m), η_0 the zero-shear viscosity and t is the sintering time (seconds). For constant particle radius and viscosity, the model is valid at early sintering stages and low shear rates [36,38]. Early research has suggested Newtonian behavior of the melt during the SLS process [38]. Bellehumer et al. [39] recognized the influence of extensional viscosity in the sintering process.

The laser sintering process is known to induce chain extensions in polyamides leading to molecular weight growth [40]. Thermal aging causes similar rheological changes as seen with photodegradation [41]. Yan et al. [33] investigated the time-dependent behavior of PEEK and CF/PEEK composites. An increase in zero-shear viscosity was associated with the post-condensation phenomenon occurring in the matrix at a temperature above T_m.

In a typical SLS print only a fraction of the total powder in the bed is incorporated into the final part and the rest ends up as powder waste, which is a drawback of this technique [39]. During SLS, the polymer powder experiences prolonged exposure to high temperatures (typically just under its melting temperature). The light transmittance of the powder governs the laser energy distribution. Tian et al. [34] considered both thermal and optical properties of neat polyamide (PA), PA/NaCl, and PA/carbon fiber (CF) composites to simulate the temperature distribution of the powder bed. Similar simulation studies were conducted of PEEK and PEEK/CF powders [33]. The temperature distribution for neat PEEK powder along the melting zone in the z-direction ranged from 350 °C to 436.17 °C and 330 °C to 350 °C within the high and low coalescence rate regions, respectively. The melting depth was reported to be 225 µm at a laser power of 10.9 W. Furthermore, the rest of the powder bed was reported to be above 300 °C. These extreme processing conditions can change the inherent chemical and physical properties of the polymer powder as described above. In early PEEK recyclability studies, concentrated sulfuric acid was used to recover the matrix from carbon fiber (APC-2) reinforced PEEK [42]. Differential scanning calorimetry (DSC) results indicated impurities present in the reclaimed matrix. Day et al. [43] observed no significant decline in viscosity average molecular weight of PEEK even after repeated injection molding cycles.

The unknown thermal history can lead to issues such as the higher amount of waste, delay in production, increased total production costs, and customer dissatisfaction. In some cases, the non-sintered (waste) powder can be reused in the same application by reprocessing it with some amount of fresh powder to avoid variation in part quality, shrinkage, and rough surface texture. To maximize the amount of powder that can be recycled, it is critical to understand the effects of temperature and heating time on PEEK powder properties and resulting behavior during the SLS process. To the best of our knowledge, no prior research on the recyclability of PEEK powders is available. The main objective of this study is to quantify changes occurring to PEEK powders during the SLS process and to predict its recyclability and processability.

2. Materials and methods

2.1. Powder details

The thermoplastic matrix selected for this study was PEEK 450PF, supplied by Victrex® plc [40]. The average particle size (D_{50}) and glass transition temperature of the powder were 50 μm and 143 °C, respectively. The manufacturer recommends drying at 120 °C for 5 h before the SLS process. To preserve the thermal history, annealed powders were characterized without pre-drying.

2.2. Thermal aging protocol

Aging was performed in batches of several hundred grams. The powder was spread in a rectangular glass pan and placed in a muffle furnace under an air atmosphere. To replicate the SLS process, aging was conducted at 330 °C and 340 °C from 2 to 12 h in 2 h increments. Fig. 2 shows the visual comparison between neat and 12 h aged PEEK powders. The aging temperatures were

Fig. 2. Unannealed (left); 12hours annealed PEEK powder (right).

selected based on numerical heat transfer simulations conducted by researchers on SLS powder beds, specifically PEEK [33].

2.3. Particle sphericity and scanning electron microscopy (SEM)

Particle morphology analysis was conducted using a Microtrac Camsizer particle analyzer (York, PA). The unannealed powder was not measured because it would not flow freely into the measurement chamber.

Microscopy was conducted using scanning electron microscopy (SEM) on a TeneoLVSEM; samples were sputter-coated with ~3 nm of gold coating to reduce surface charging. Microscopy was performed to investigate the microstructure of powder before and after annealing.

2.4. Differential scanning calorimetry (DSC) and thermogravimetric analysis (TGA)

Differential scanning calorimetry (DSC), TA Instruments, Discovery series), and thermogravimetric analysis (TGA), TA Instruments, Discovery series) were used to characterize glass transition temperature (T_g), melting temperature (T_m), and degradation characteristics of PEEK. All measurements were performed under a nitrogen atmosphere. A heat, cool, and heat procedure was incorporated according to ASTM D3418 for DSC: ramp to 400 °C at 20 °C/min, isotherm at 400 °C for 2 min, cool to 0 °C at 20 °C/min, isotherm for 2 min, ramp to 400 °C at 20 °C/min. Percent crystallinity (%X) was calculated from the melting endotherms using Eq (2):

$$\%X = \frac{(\Delta H_{f^o})}{\Delta H_{f(100\%)}} \times 100\% \quad (2)$$

Here $\Delta H_{f(100\%)}$ is the melting enthalpy of 100% crystalline PEEK: 130 Jg^{-1} [44]. TGA was carried out under air environment. Samples were heated at a ramp rate of 10 °C/min, from 0 °C to 995 °C in synthetic air (20% O_2/80% N_2). Initial weight loss at 100 °C was attributed to the loss of moisture or water. The onset temperature was defined as the intersection point of the extrapolated baseline and the tangent of the inflection point. Measurements were repeated a total of three times for each sample.

2.5. Fourier transform infrared spectroscopy (FTIR)

Fourier transform infrared (FTIR) FTIR spectra of the powders were measured with a Nicolet iS650 FTIR Spectrometer using ATR (attenuated total reflectance) mode in the wavenumber range 400 to 4000cm^{-1} with a resolution of 4 cm^{-1} and averaging 64 scans. Measurements were performed using PEEK powders, and the results were an average of three measurements.

2.6. X-ray diffraction (XRD)

X-ray diffraction (XRD) was used to characterize the crystalline properties of various PEEK samples, including the effects of process aging on material crystalline ratios and crystal sizes. XRD was performed using a D2 Phaser diffractometer (Bruker, Germany) with CuKα radiation (λ =1.54060 Å) on PEEK samples (including new powders, powders aged at 330 °C with different aging time, and powders aged at 340 °C with different aging time). Sample crystalline ratios were obtained directly from analyzing the XRD patterns with distinguished crystalline region and amorphous region. Sample crystallite sizes were calculated according to the Scherrer equation (Eq. (3)). L is the crystal size, nm. K is the Scherrer constant. λ is the X-ray wavelength. FW(2θ) is the width of the diffraction peak in radians, at a height half-way between background and the peak maximum. θ is the Bragg angle.

$$L = \frac{K\lambda}{FW(2\theta)cos\theta} \quad (3)$$

2.7. Small-angle oscillatory shear (SAOS) rheology

Parallel plate melt rheology was conducted on an ARES-G2 rheometer (TA instruments, New Castle, DE) with 8 mm stainless steel plates. disk samples were compression molded from PEEK powders that were vacuum dried at 120 °C for 5 h. Frequency sweeps were performed at 380 °C over 0.1–100 rad/s using a 5% strain (previously determined to be within the linear viscoelastic region). Each sample was equilibrated for 30 s before the gap was set to the testing position (approximately 1.2 mm) or until the top plate contacted the top surface of the sample. Complex viscosity (Pa.s) was measured within the frequency range of 0.1 to 100 rad/*sec*.

2.8. Angle of repose (AOR)

Prediction of performance during processing was investigated using powder flow tester and SLS printing trials. The angle of repose testing was performed using a powder flowability tester (Gardco, Inc.) following ASTM D6393.

3. Results and discussion

Observations on the morphology, chemical, thermal, and rheological changes provided most of the experimental evidence in this

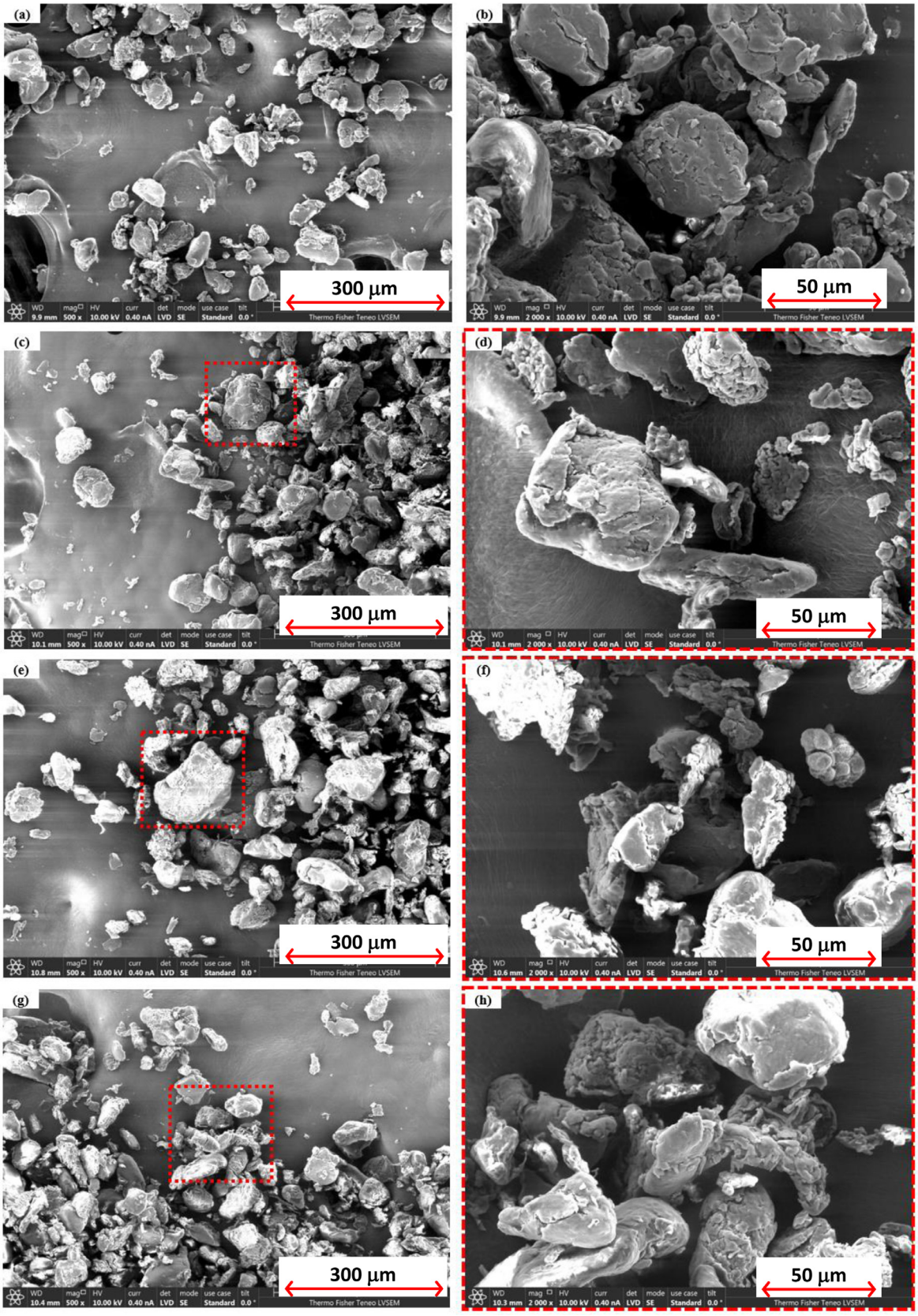

Fig. 3. SEM images for PEEK **(a), (b)** virgin powder, **(c), (d)** aging conducted at 330 °C, 2 h, **(e), (f)** aging conducted at 330 °C, 6 h, **(g), (h)** aging conducted at 330 °C, 12 h. SEM images on the left are of lower magnification, and images on the right are of higher magnification.

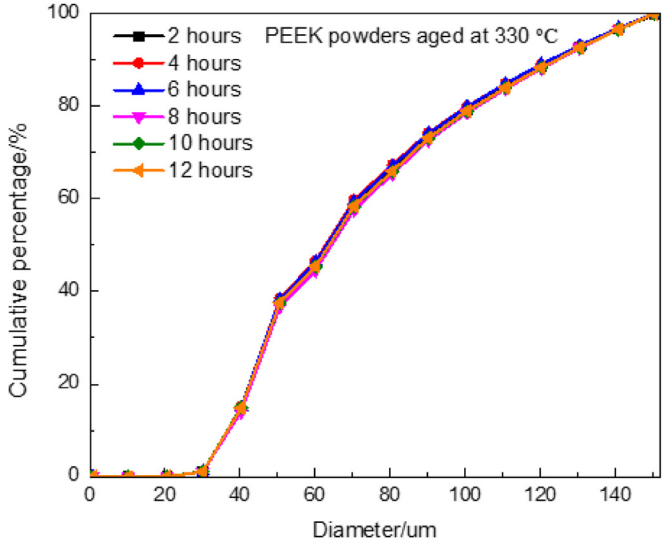

Fig. 4. Particle size distribution for virgin PEEK and aged PEEK between 2 and 12 h.

study. It should be noted that molecular weight was not directly measured in this study, which would be helpful for understanding the nature of chemical changes.

3.1. Physical characteristics and morphology of peek powder

Considering both the temperature distribution reported in literature and sintering time for PEEK, study of thermal aging at 330 °C and 340 °C was conducted for two-hour intervals up to a cumulative 24 h. As shown in Fig. 2, the powders became slightly yellowed after this period of thermal annealing.

The particle morphology of virgin and aged PEEK powders at lower (left) and higher (right) magnifications are shown in Fig. 3. The morphology of virgin PEEK 450 PF appears irregular with the presence of fibrillated structures on the surface. This irregular shape is known to induce inter-particle friction inhibiting the flow properties of the powder. As shown in Fig. 3(c) to (h), after annealing, no substantive changes in the particle surface or morphology could be observed. Results shown here are only for 330 °C because the observations for powders annealed at 340 °C were similar.

Table 1
Sphericity values for virgin and aged powders.

Percentage of particle sphericity from 0.85 to 1.0%		Percentage increase from 2 to 12 h
330 °C 2 h	43%	3.66±1.2%
330 °C 4 h	45%	
330 °C 6 h	45%	
330 °C 8 h	46%	
330 °C 10 h	46%	
330 °C 12 h	47%	

The sphericity of a particle is one of the fundamental physical characteristics of the powder. Powder size and shape analysis were conducted on samples annealed up to 12 h for 330 °C annealing; sphericity measurements on the annealed powders were repeated three times and the average and standard deviation of the percent increase from 2 to 12 h was calculated. Table 1 shows that the sphericity values for PEEK 450 PF powder increase slightly, but with statistical significance.

Both aged and unaged PEEK powders exhibit similar PSD, as shown in Fig. 4. The cumulative percentage of particles at a given diameter was not shown to change for any of the times or temperatures. Repeats of the PSD measurements did not reveal any significant trend in the PSD over isothermal aging of the powders at 330 °C or 340 °C.

3.2. Melt rheology

Eq. (1) suggests the powder coalescence rates are inversely related to zero-shear viscosity of the matrix. As for most thermoplastics, neat and aged PEEK portray shear thinning behavior. To understand the real-time behavior of the SLS powders, we performed viscosity measurements at low shear rates; the complex viscosity at a frequency of 0.1 rad/s is estimated as zero-shear viscosity in this study. From Fig. 5(a), the difference in flow behavior between virgin and aged PEEK is noticeable. Both aged samples show steeper shear thinning than the virgin PEEK. The 12 hour

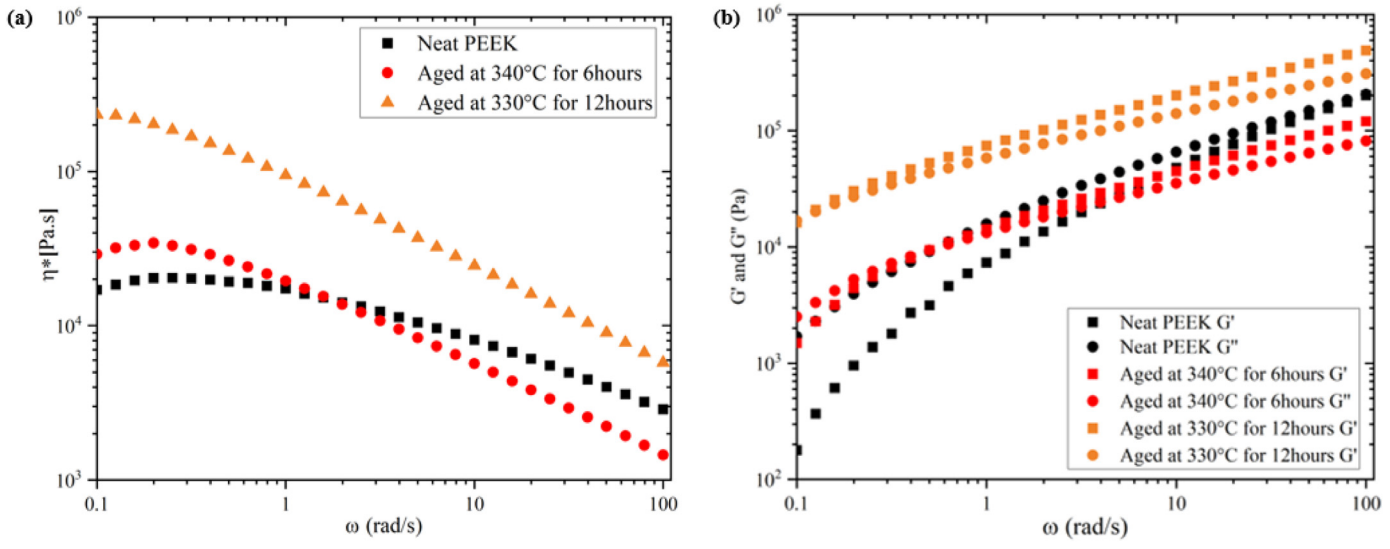

Fig. 5. variation of **(a)** complex viscosity, and **(b)** storage (G'), loss modulus (G") with the increase in oscillatory frequency at 380 °C.

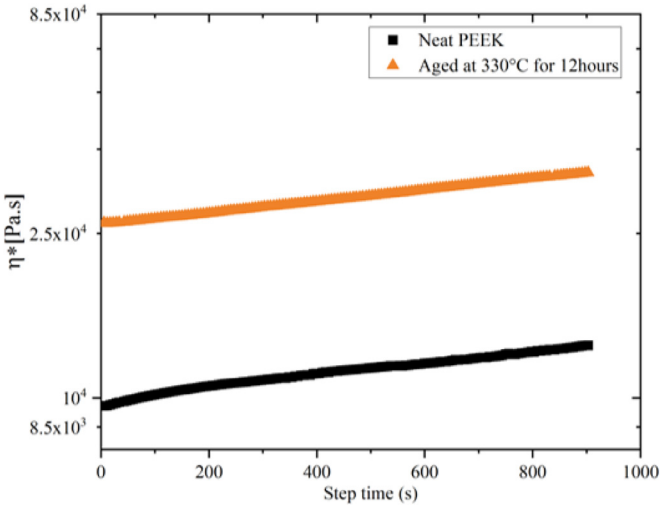

Fig. 6. Time-dependent behavior of viscoelastic parameters (storage (G') and loss (G") modulus) for neat and aged PEEK at 10 rad/s and 380 °C.

aged sample shows higher viscosity throughout the entire low-frequency regime. The aged samples also have a higher storage modulus with less dependence on frequency, indicating more elasticity compared to the untreated PEEK. The crossover of the storage and loss modulus (Fig. 5(b)) occurs at lower frequency for both aged samples, indicating formation of network-like structure due to higher molecular weight or increased branching.

In Fig. 6, the increase in complex viscosity with time was associated with the post-condensation phenomenon occurring in the melt at a temperature above T_m (360 °C). This increase with time could also be responsible for the slight maximum observed at low frequency during the frequency sweep shown in Fig. 5; the data points in the first frequency decade take around ten minutes to collect, while the entire test only takes about 12 min.

3.3. FTIR

The carbonyl group ($C = O$) peak within the regime 1540–1870 cm^{-1} was not affected under aging conditions, suggesting the absence of chemical degradation in PEEK powders (Fig. 7). Hydroxyl group (-OH) absorption at (2800–3700cm^{-1}) may broaden with the aging of PEEK powder, which is also insignificant at the 330 °C aging condition. Similar observations were made for the powders at 340 °C. Previous research on PEEK fibers suggested significant growth in the $C = O$ peak affiliated with carboxylic acids (specifically around 1740 cm^{-1}) with long term aging from 1 to 128 days at 250 °C [27]. As shown in the insets of Fig. 7 (bottom right), the FTIR spectra did not indicate chemical changes to either the -OH peak or the carbonyl peak.

3.4. Thermal analysis: dsc and tga

Annealing studies on PEEK have previously demonstrated increased crystallinity and Young's modulus [27]. However, crosslink-

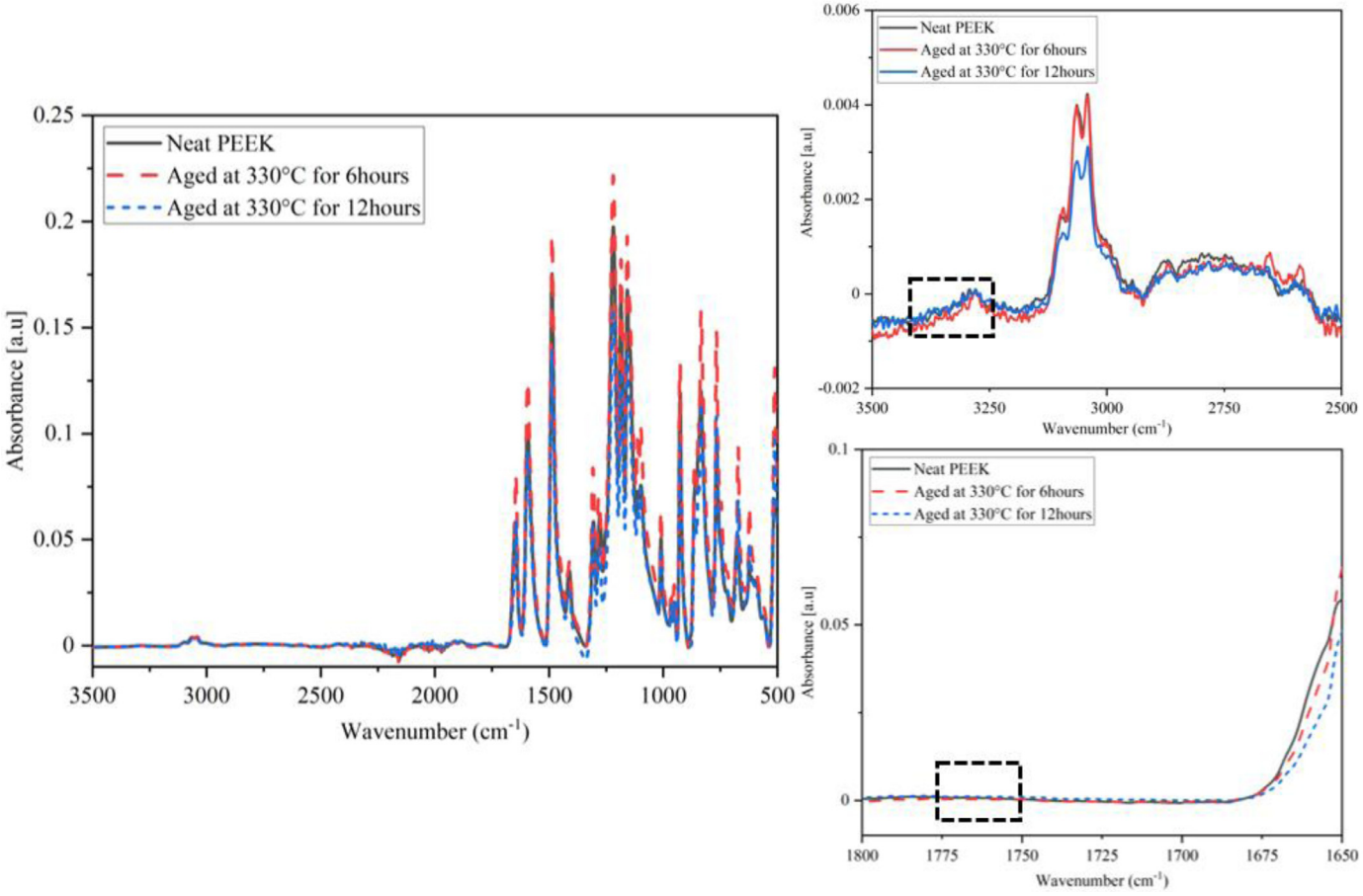

Fig. 7. FTIR spectra, hydroxyl region (top right), and carbonyl (bottom right), and for neat and aged PEEK. Black dashed box shows the specific peak regions where changes to -OH and $C = O$ could be expected.

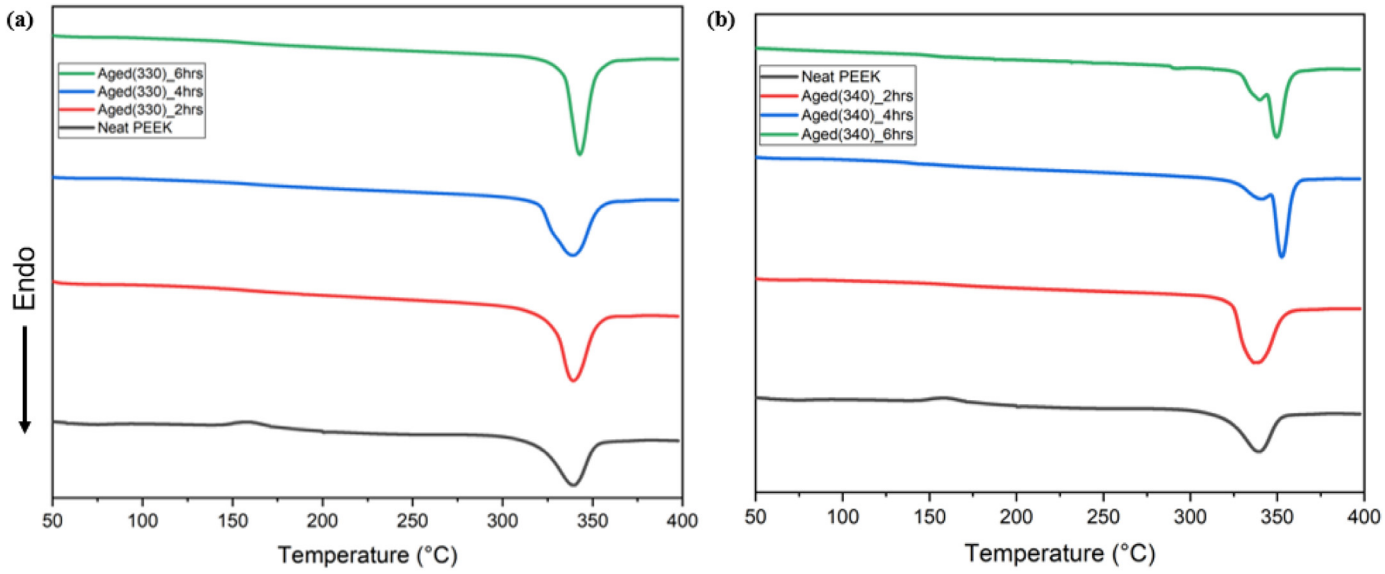

Fig. 8. DSC thermograms for neat and thermally aged PEEK powders during the first heating cycle **(a)** 330 °C, **(b)** 340 °C.

Table 2
Glass transition, melting temperature, and crystallinity data for neat and aged PEEK.

Sample Name	Tg_1 (°C)	Tg_2 (°C)	Tm_1-Peak(°C)	Tm_2-Peak (°C)	Tm_1–Onset(°C)	Tm_2-onset (°C)	$\%X_1$	$\%X_2$
Neat PEEK	149.60± 2.1	151.91±2.12	339.27±.35	339.96±0.40	325.58±9.40	331.11±7.93	47.83±5.77	30.15±2.00
PEEK Aged 330 °C 2hrs	149.07±3.8	149.70±0.27	343.60±6.59	340.29±0.20	335.55±8.45	326.56±0.21	51.03±2.90	31.29±.89
PEEK Aged 330 °C 4hrs	144.50±1.1	149.84±0.71	338.40±0.43	340.59±.51	324.23±4.15	329.30±4.81	57.41±2.62	32.94±0.84
PEEK Aged 330 °C 12hrs	146.64±2.60	150.18±0.16	344.94±5.29	340.62±0.06	336.95±6.91	326.63±0.91	53.44±2.01	32.56±1.16
Sample Name	Tg_1 (°C)	Tg_2 (°C)	Tm_1-Peak(°C)	Tm_2-Peak (°C)	Tm_1–Onset(°C)	Tm_2-onset (°C)	$\%X_1$	$\%X_2$
PEEK Aged 340 °C 2hrs	145.82±1.5	151.10±1.15	340.81±5.69	340.37±0.73	331.38±8.11	328.39±3.20	52.46±4.72	32.17±0.79
PEEK Aged 340 °C 6hrs	149.16±0.9	149.87±0.81	349.09±4.84	340.45±0.23	341.49±5.86	326.37±2.30	50.86±1.38	33.19±2.44
PEEK Aged 340 °C 12hrs	141.91±1.6	150.44±0.68	349.89±1.37	339.88±1.25	342.88±1.54	326.23±0.93	52.33±1.35	32.09±0.87

NOTE: Subscript 1 and 2 refer to the first and second heating cycles, respectively.

ing occurring in the matrix at temperatures above 290 °C reduced molecular mobility, thus inhibiting annealing and further causing decreased crystallinity and Young's modulus. DSC thermograms of the first heating cycle for virgin and annealed PEEK are shown in Fig. 8. A secondary melting endotherm appears at a higher temperature than the main melting peak, especially clear in the 4 and 6 hour aged samples at 340 °C. With the thermal history being eliminated under the second heating cycle, no trace of the secondary endothermic peak was observed for PEEK at the aging temperatures (not shown). Percent crystallinity (%X) was determined from the melting endotherms for both the first and second heat using Eq (2).

Table 2 shows the thermal characteristics of neat PEEK and the effect of aging. The melting point of the neat polymer is observed to be 329 °C, and the aging of the powders has no recordable effect on the T_m, suggesting the absence of any bulk degradation of the polymer matrix. Also, no noteworthy trend in T_g was observed, indicating limited changes to molecular architecture such as crosslinking occurring during isothermal aging. A slight increase in crystallinity measured from the first heat was observed, though it was barely statistically significant beyond sample-to-sample variation.

It has been previously reported that thermal aging of PEEK reduces its thermal stability [27]. However, the thermal stability of PEEK powders aged from 2 to 6 h was similar to neat PEEK (Figs. 9 and 10). PEEK aged for 2 h showed slightly faster first and second stage decomposition rates compared to others (Figs. 9 and 10(b) and (c)), which could not be explained within the context of this study. Repeated TGA tests were conducted to try to determine the reason for faster degradation of the 2-hour sample. The variability in the data across different samples from the same annealing batch conditions showed that this slight early weight loss was repeatable but very minor.

3.5. X-ray diffraction

All the specimens were analyzed for crystallinity using X-ray diffraction to confirm the trends shown by DSC. The percent crystallinity deduced from XRD in Fig. 10 shows an apparent increase for all PEEK powders annealed for as little as one hour. The% crystallinity values presented are from fits to the amorphous and crystalline peaks, represented in the diffractogram shown in Fig. 10(a). The growth in crystallinity appears to continue for the first several hours of annealing at 330 °C, but repeated measurements reveal that they are within experimental error. After two hours of annealing, an average equilibrium value of 35.7 ± 0.6% is reached. The annealing at 340 °C increases the PEEK crystallinity a similar amount, and the process is complete after two hours. The crystal size data in Fig. 10(c) show a more systematic increase, typical for semi-crystalline polymers that can re-

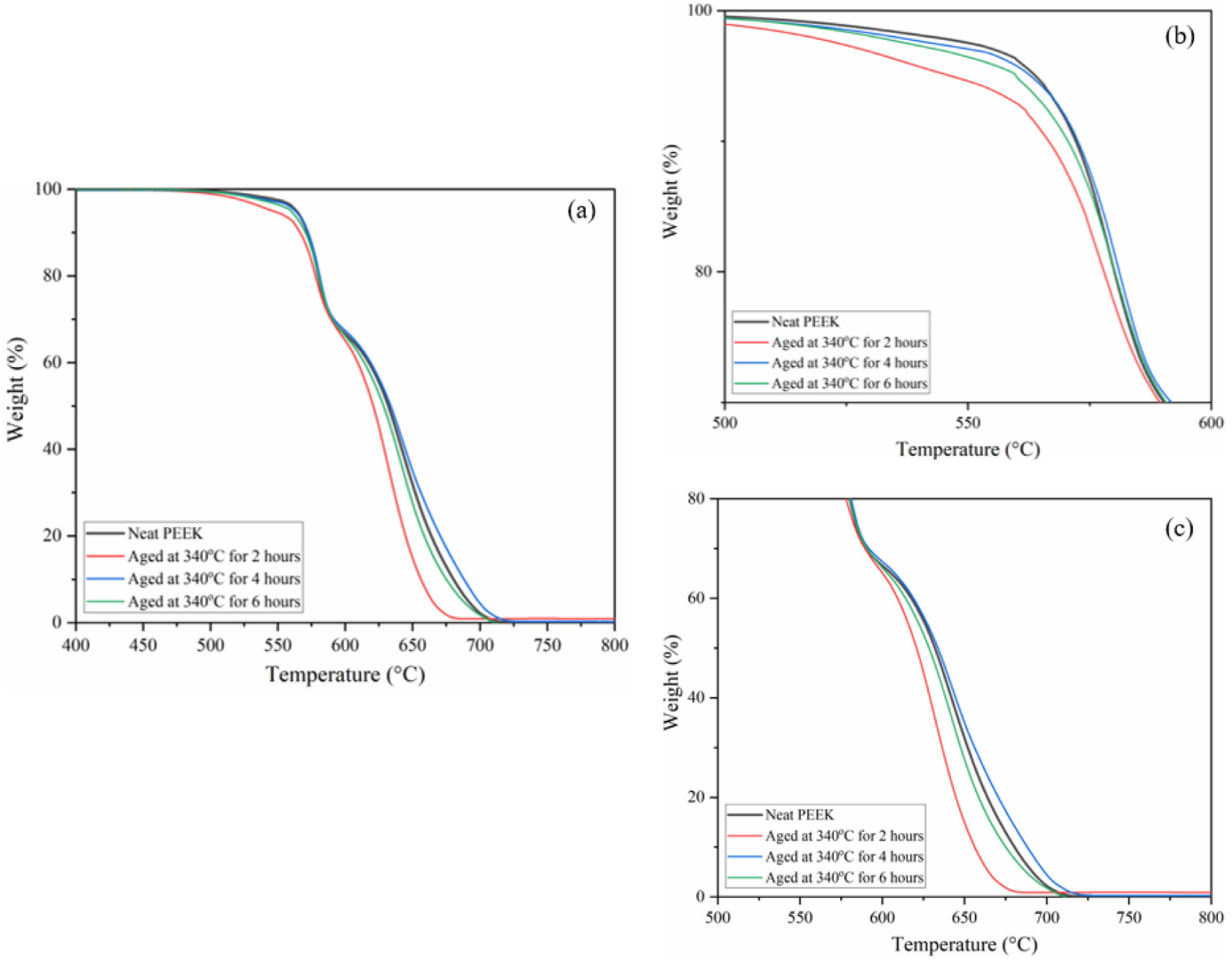

Fig. 9. **(a)** TGA thermograms for neat and thermally aged (at 340 °C) PEEK powders; **(b)** first decomposition region; **(b)** second decomposition region. The trends of weight loss with temperature were similar for powders aged at 330 °C.

Table 3
Angle of repose measurements for neat and aged PEEK powders.

Sample Name	The angle of repose (degrees)	Comment
Virgin PEEK-dried	50.87±0.24	Poor- must agitate, vibrate
PEEK Aged @ 330 °C 4hrs	48.65±0.18	
PEEK Aged @ 330 °C 8hrs	49.20±0.09	

organize into larger and more perfect crystals under annealing conditions.

3.6. Angle of repose

From the observation during particle size analysis that the neat powders did not flow smoothly, powder flowability was tested using ASTM D6393, a standard test method for bulk solids characterization by Carr Indices. This method requires a special apparatus that consists of a steel funnel, a tapping or stirring device, and a flat platform from which one measures the sloping angle that the powder makes after flowing from the funnel to the platform (Fig. 10).

The angle of repose of SLS powders were determined using Eq. (4):

$$\theta = \tan^{-1}\left(\frac{Height\ of\ cone\ (mm)}{50\ mm}\right) \quad (4)$$

The standard states that if the powder mound forms an angle lower than 40°, the powder will likely move without assistance in processes requiring free flow. Angles larger than 46° are considered poor flowability, and assistance such as vibration will be required for powder transport. As shown in Table 3, the Angle of Repose test gave angles in the “poor” regime for all powders in this study, as received and annealed. The value slightly decreases for annealed powders, but this is not a large enough difference to explain the

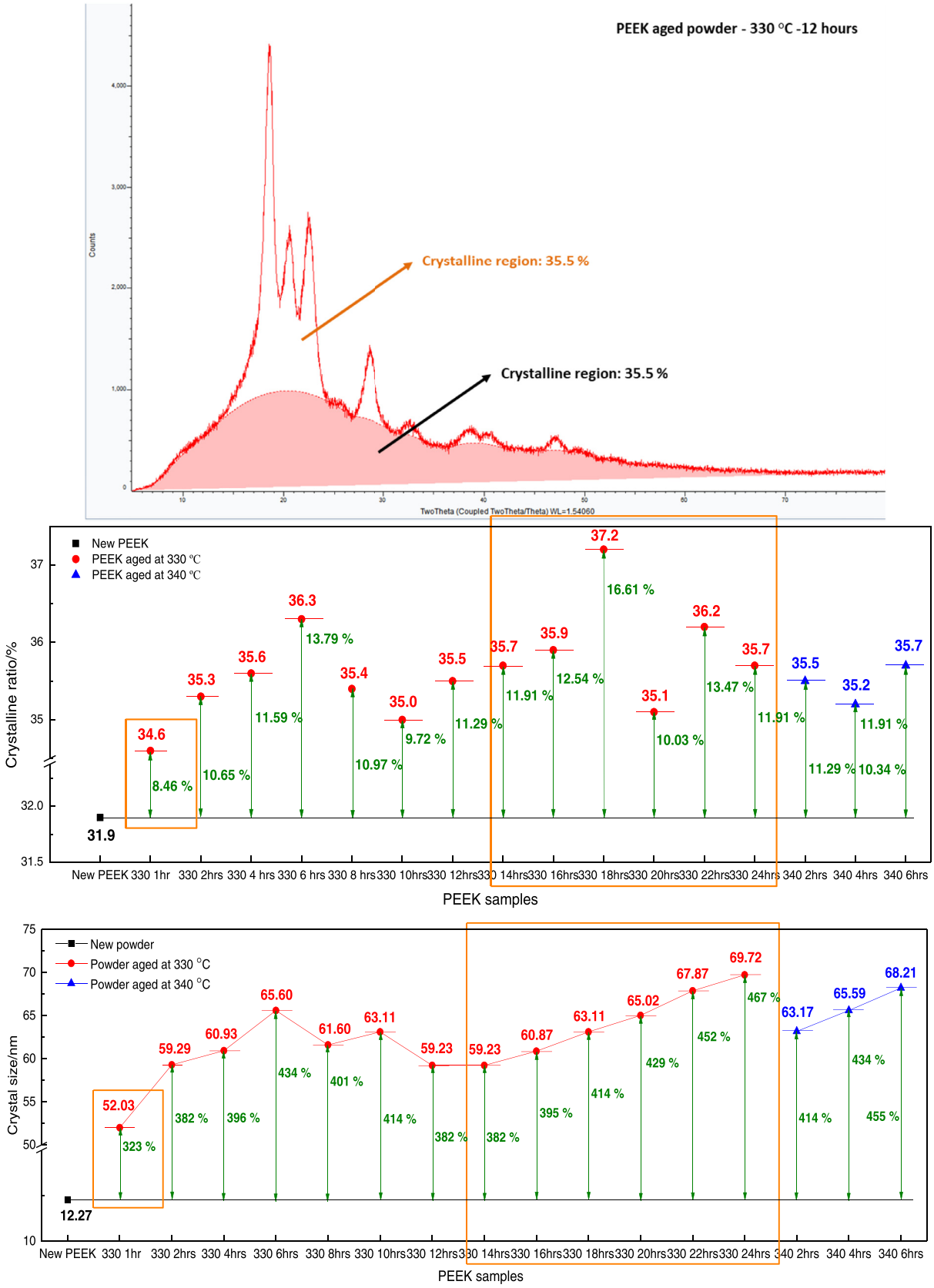

Fig. 10. **(a)** example XRD diffractogram for PEEK powder showing the shaded broad, amorphous peak and the crystal peak reflections; **(b)** analysis of percent crystallinity and (c) crystal size for all annealed samples.

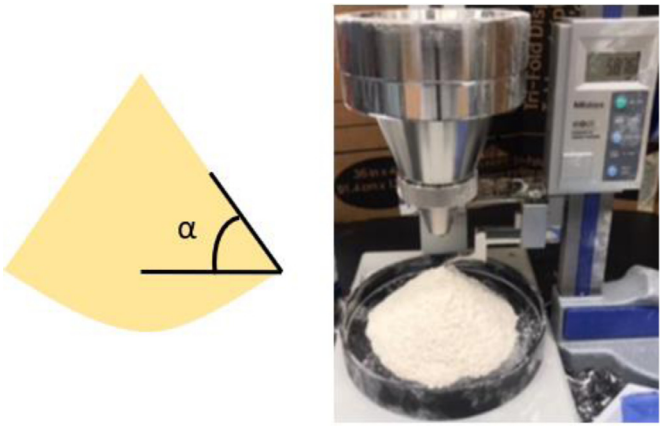

Fig. 11. (left) Steepest angle made by the SLS powder with the horizontal plane; (right) Gardco angle of repose apparatus.

difference seen in the particle size analyzer. Further investigation is required to justify that this difference would result in any changes for the SLS process, where a spreader bar is used to distribute each layer of powder. Additional testing is recommended (e.g., Ring Shear Cell, ASTM D6773) determine if spreadability would be affected.

4. Conclusion

This work investigated the changes in several thermophysical properties of PEEK powders used in SLS to understand the influence of powder bed environmental conditions on powder aging. No specific chemical changes such as oxidation were observed using FTIR, though rheological results indicated molecular weight growth or branching occurred. While morphological observations of the powder's shape, size and surface did not indicate significant differences upon thermal aging, rheological, scattering and thermal measurements indicated that in the most significant changes in the polymer were to molecular weight and crystalline structure. The crystallinity increase, while modest, could have significant effects on the sintering behavior if less amorphous material is available to diffuse among adjacent particles. The increased zero-shear viscosity and elasticity are predicted to slow the sintering process for PEEK powder that has been thermally aged. The rheological findings shown herein could be combined with Eq. (1) to modify SLS process parameters to consider the slower sintering of recycled PEEK power, or to incorporate enough virgin powder to counteract the behavior. The flowability of the powder did increase after annealing (as evidenced by the particle size measurement difficulty before annealing), but the angle of repose test method did not prove sensitive enough to distinguish this behavior quantitatively. This materials study will be complemented in future work with SLS test prints and evaluation of mechanical properties to link changes to part quality with the thermal history of the powder. The combination of structure, property and processing characterizations presented here will be useful in creating a roadmap for incorporation of recycled PEEK powder in SLS processes, which will eliminate waste and save cost.

Declaration of Competing Interest

The authors declare that they have no known competing financial interests or personal relationships that could have appeared to influence the work reported in this paper.

CRediT authorship contribution statement

Akanksha Patel: Data curation. **Varun Venoor:** Data curation, Formal analysis, Methodology. **FeiFei Yang:** Methodology, Data curation, Formal analysis. **Xu Chen:** Conceptualization, Formal analysis, Funding acquisition, Methodology, Project administration. **Margaret J. Sobkowicz:** Conceptualization, Formal analysis, Funding acquisition, Methodology, Project administration, Writing - review & editing.

Acknowledgments

This material is based upon work supported by the National Science Foundation under grant number IIP-1822147 (Phase I IUCRC at University of Massachusetts Lowell: Center for Science of Heterogeneous Additive Printing of 3D Materials (SHAP3D)) and from the SHAP3D I/UCRC Members: Boeing Company, U.S. Army CCDC Soldier Center, Desktop Metal, HP Inc, Hutchinson, Integrity Industrial Ink Jet Integration LLC, Raytheon Technologies, Stratasys Ltd, and Triton Systems Inc. Any opinions, findings, and conclusions or recommendations expressed in this material are those of the author(s) and do not necessarily reflect the views of the National Science Foundation or the sponsors.

Supplementary materials

Supplementary material associated with this article can be found, in the online version, at doi:10.1016/j.polymdegradstab.2021.109502.

References

[1] T.D. Ngo, A. Kashani, G. Imbalzano, K.T.Q. Nguyen, D. Hui, Additive manufacturing (3D printing): a review of materials, methods, applications and challenges, Compos. Part B Eng. 143 (2018) 172–196, doi:10.1016/j.compositesb.2018.02.012.
[2] J. O'Donnell, F. Ahmadkhanlou, H.-.S. Yoon, G. Washington, All-printed smart structures: a viable option? Act. Passive Smart Struct. Integr. Syst. 2014, International Society for Optics and Photonics, 2014, doi:10.1117/12.2045284.
[3] S. Ahn, M. Montero, D. Odell, S. Roundy, P.K. Wright, Anisotropic material properties of fused deposition modeling ABS, Rapid Prototyp. J. 8 (2002) 248–257, doi:10.1108/13552540210441166.
[4] A.R. Zanjanijam, I. Major, J.G. Lyons, U. Lafont, D.M. Devine, Fused Filament Fabrication of PEEK: a Review of Process-Structure-Property Relationships, Polymers (Basel) 12 (2020), doi:10.3390/polym12081665.
[5] A. Manthiram, H.L. Marcus, D.L. Bourell, Selective laser sintering using nanocomposite materials, U.S. Patent No. 5,431,967, 1995.
[6] E. Berry, J.M. Brown, M. Connell, C.M. Craven, N.D. Efford, A. Radjenovic, M.A. Smith, Preliminary experience with medical applications of rapid prototyping by selective laser sintering, Med. Eng. Phys. 19 (1997) 90–96, doi:10.1016/S1350-4533(96)00039-2.
[7] J.-.P. Kruth, X. Wang, T. Laoui, L. Froyen, Lasers and materials in selective laser sintering, Assem. Autom. (2003).
[8] M. Zalaznik, M. Kalin, S. Novak, Influence of the processing temperature on the tribological and mechanical properties of poly-ether-ether-ketone (PEEK) polymer, Tribol. Int. 94 (2016) 92–97.
[9] G.H. Melton, E.N. Peters, R.K. Arisman, 2 - Engineering Thermoplastics, in: M. Kutz (Ed.), Appl. Plast. Eng. Handb., William Andrew Publishing, Oxford, 2011, pp. 7–21, doi:10.1016/B978-1-4377-3514-7.10002-9.
[10] M. Garcia-Leiner, M.T. Reitman, M.J. El-Hibri, R.K. Roeder, Structure-property relationships in commercial polyetheretherketone resins, Polym. Eng. Sci. 57 (2017) 955–964.
[11] T.L. Conrad, D.J. Jaekel, S.M. Kurtz, R.K. Roeder, Effects of the mold temperature on the mechanical properties and crystallinity of hydroxyapatite whisker-reinforced polyetheretherketone scaffolds, J. Biomed. Mater. Res. B Appl. Biomater. 101 (2013) 576–583.
[12] M. Roskies, J.O. Jordan, D. Fang, M.-.N. Abdallah, M.P. Hier, A. Mlynarek, F. Tamimi, S.D. Tran, Improving PEEK bioactivity for craniofacial reconstruction using a 3D printed scaffold embedded with mesenchymal stem cells, J. Biomater. Appl. 31 (2016) 132–139.
[13] R.K. Roeder, Bioactive Polyaryletherketone Composites, in: PEEK Biomater. Handb., Elsevier, 2019, pp. 203–227, doi:10.1016/B978-0-12-812524-3.00012-0.
[14] C. Basgul, T. Yu, D.W. MacDonald, R. Siskey, M. Marcolongo, S.M. Kurtz, Structure-Property Relationships for 3D printed PEEK Intervertebral Lumbar Cages Produced using Fused Filament Fabrication, J. Mater. Res. 33 (2018) 2040–2051, doi:10.1557/jmr.2018.178.

[15] M. Vaezi, S. Yang, Extrusion-based additive manufacturing of PEEK for biomedical applications, Virtual Phys. Prototyp. 10 (2015) 123–135, doi:10.1080/17452759.2015.1097053.
[16] S. Ziegelmeier, F. Wöllecke, C. Tuck, R. Goodridge, R. Hague, Characterizing the bulk & flow behaviour of LS polymer powders, in: Proc. SFF Symp, Austin TX USA, 2013.
[17] S. Yuan, F. Shen, C.K. Chua, K. Zhou, Polymeric composites for powder-based additive manufacturing: materials and applications, Prog. Polym. Sci. 91 (2019) 141–168, doi:10.1016/j.progpolymsci.2018.11.001.
[18] R.D. Goodridge, C.J. Tuck, R.J.M. Hague, Laser sintering of polyamides and other polymers, Prog. Mater. Sci. 57 (2012) 229–267.
[19] J.P. Schultz, J.P. Martin, R.G. Kander, C.T. Suchicital, Selective laser sintering of nylon 12-PEEK blends formed by cryogenic mechanical alloying, 2000 Int. Solid Free. Fabr. Symp., 2000.
[20] J.K. Prescott, R.A. Barnum, On powder flowability, Pharm. Technol. 24 (2000) 60–85.
[21] D. Schulze, Flow properties of powders and bulk solids, Braunschweig-Wolfenbu Ttel Ger. Univ. Appl. Sci. (2006).
[22] H. Chung, S. Das, Processing and properties of glass bead particulate-filled functionally graded Nylon-11 composites produced by selective laser sintering, Mater. Sci. Eng. A. 437 (2006) 226–234.
[23] I. Gibson, D. Shi, Material properties and fabrication parameters in selective laser sintering process, Rapid Prototyp. J. 3 (1997) 129–136, doi:10.1108/13552549710191836.
[24] S. Berretta, O. Ghita, K.E. Evans, Morphology of polymeric powders in Laser Sintering (LS): from Polyamide to new PEEK powders, Eur. Polym. J. 59 (2014) 218–229, doi:10.1016/j.eurpolymj.2014.08.004.
[25] A. Jonas, R. Legras, Thermal stability and crystallization of poly(aryl ether ether ketone), Polymer (Guildf) 32 (1991) 2691–2706, doi:10.1016/0032-3861(91)90095-Z.
[26] M.T. Bishop, F.E. Karasz, P.S. Russo, K.H. Langley, Solubility and properties of a poly (aryl ether ketone) in strong acids, Macromolecules 18 (1985) 86–93.
[27] V. Mylläri, T.-.P. Ruoko, J. Vuorinen, H. Lemmetyinen, Characterization of thermally aged polyetheretherketone fibres–mechanical, thermal, rheological and chemical property changes, Polym. Degrad. Stab. 120 (2015) 419–426.
[28] P. Patel, T.R. Hull, R.W. McCabe, D. Flath, J. Grasmeder, M. Percy, Mechanism of thermal decomposition of poly (ether ether ketone)(PEEK) from a review of decomposition studies, Polym. Degrad. Stab. 95 (2010) 709–718.
[29] C.J. Tsai, L.H. Perng, Y.C. Ling, A study of thermal degradation of poly (aryl-ether-ether-ketone) using stepwise pyrolysis/gas chromatography/mass spectrometry, Rapid Commun. Mass Spectrom. 11 (1997) 1987–1995.
[30] K.C. Cole, I.G. Casella, Fourier transform infrared spectroscopic study of thermal degradation in films of poly(etheretherketone), Thermochim. Acta. 211 (1992) 209–228, doi:10.1016/0040-6031(92)87021-2.
[31] M. Day, D. Sally, D.M. Wiles, Thermal degradation of poly(aryl-ether-ether-ketone): experimental evaluation of crosslinking reactions, J. Appl. Polym. Sci. 40 (1990) 1615–1625, doi:10.1002/app.1990.070400917.
[32] J.N. Hay, D.J. Kemmish, Thermal decomposition of poly(aryl ether ketones), Polymer (Guildf) 28 (1987) 2047–2051, doi:10.1016/0032-3861(87)90039-5.
[33] M. Yan, X. Tian, G. Peng, D. Li, X. Zhang, High temperature rheological behavior and sintering kinetics of CF/PEEK composites during selective laser sintering, Compos. Sci. Technol. 165 (2018) 140–147, doi:10.1016/j.compscitech.2018.06.023.
[34] X. Tian, G. Peng, M. Yan, S. He, R. Yao, Process prediction of selective laser sintering based on heat transfer analysis for polyamide composite powders, Int. J. Heat Mass Transf. 120 (2018) 379–386, doi:10.1016/j.ijheatmasstransfer.2017.12.045.
[35] PA 12 - PA2200: Nylon for Industrial 3D Printing \textbar EOS GmbH, n.d. https://www.eos.info/en/additive-manufacturing/3d-printing-plastic/sls-polymer-materials/polyamide-pa-12-alumide (accessed October 12, 2020).
[36] B. Haworth, N. Hopkinson, D. Hitt, X. Zhong, Shear viscosity measurements on Polyamide-12 polymers for laser sintering, Rapid Prototyp. J. 19 (2013) 28–36, doi:10.1108/13552541311292709.
[37] J. Bai, R.D. Goodridge, R.J.M. Hague, M. Song, M. Okamoto, Influence of carbon nanotubes on the rheology and dynamic mechanical properties of polyamide-12 for laser sintering, Polym. Test. 36 (2014) 95–100, doi:10.1016/j.polymertesting.2014.03.012.
[38] J.-.D. Muller, M. Bousmina, A. Maazouz, 2D-Sintering Kinetics of Two Model Fluids as Drops, Macromolecules 41 (2008) 2096–2103, doi:10.1021/ma702349s.
[39] C.T. Bellehumeur, M.K. Bisaria, J. Vlachopoulos, An experimental study and model assessment of polymer sintering, Polym. Eng. Sci. 36 (1996) 2198–2207, doi:10.1002/pen.10617.
[40] C.T. Bellehumeur, M. Kontopoulou, J. Vlachopoulos, The role of viscoelasticity in polymer sintering, Rheol. Acta. 37 (1998) 270–278, doi:10.1007/s003970050114.
[41] H. Zarringhalam, N. Hopkinson, N.F. Kamperman, J.J. de Vlieger, Effects of processing on microstructure and properties of SLS Nylon 12, Mater. Sci. Eng. A. 435-436 (2006) 172–180, doi:10.1016/j.msea.2006.07.084.
[42] M. Buggy, L. Farragher, W. Madden, Recycling of composite materials, J. Mater. Process. Technol. 55 (1995) 448–456, doi:10.1016/0924-0136(95)02037-3.
[43] R.J. Day, A.K. Wood, S.F. Pang, Recycling of APC-2 offcuts, Compos. Manuf. 5 (1994) 187–193, doi:10.1016/0956-7143(94)90028-0.
[44] E. Courvoisier, Y. Bicaba, X. Colin, Multi-scale and multi-technique analysis of the thermal degradation of poly(ether ether ketone), Polym. Degrad. Stab. 151 (2018) 65–79, doi:10.1016/j.polymdegradstab.2018.03.001.